Journal of GeoEngineering, Vol. 15, No. 1, pp. 13-29, March 2020
http://dx.doi.org/10.6310/jog.202003_15(1).2

PERFORMANCE OF GEOSYNTHETIC-REINFORCED SOIL WALLS AT FAILURE

Wen-Yi Hung [1], Kuo-Hsin Yang [2*], Thanh Son Nguyen [3], and Truong-Nhat-Phuong Pham [4]

ABSTRACT

A series of centrifuge tests was conducted to investigate the performance of geosynthetic-reinforced soil (GRS) walls under failure conditions and evaluate the applicability of limit equilibrium (LE) analysis for the internal stability design of GRS walls. The test variables were reinforcement material and wall height. The failure process, failure mode, and wall facing displacement were observed and discussed. The test results revealed that the wall deformed gradually as the applied *g*-level increased. At pre-failure stage, excessive settlement occurred close to the wall crest, and a distinct subsidence developed at the top of the wall at the end of the reinforced zone. At the moment of failure, wall deformation suddenly increased, and the wall collapsed instantly. The location of the critical failure surface of the GRS wall was affected by the reinforcement inclusion. The upper limit of the critical failure surfaces of all tests was bounded by Rankine's theory. Back-calculation from the centrifuge test results revealed that all the wall models with different reinforcement and wall geometric parameters yielded a single equivalent earth pressure coefficient K_T, and the K_T value was comparable to theoretical active earth pressure coefficients. The failure *g*-level and location of the critical failure surface predicted by LE analyses were in good agreement with the observed ones from centrifuge tests, validating the applicability of LE analysis as a basis for the internal design of GRS walls. On the basis of the established relationship between the factor of safety and wall facing displacement, the inherent factors of safety ranged from FSs = 1.5 to 2.5 for the wall deformation under serviceability conditions, as suggested in several design guidelines. The maximum horizontal facing displacement reached 8% ~ 12% of the wall height at incipient wall failure. Compared with the wall deformation data in the literature, the global reinforcement stiffness was observed to have a significant influence on the maximum horizontal facing displacement of GRS walls at failure.

Key words: Geosynthetic-reinforced soil wall, centrifuge test, failure, limit equilibrium, facing deformation.

1. INTRODUCTION

Geosynthetic-reinforced soil (GRS) structures have been widely applied in various construction projects, including foundations, highway embankments, bridge abutments, and slope stabilization. GRS structures have also been used as a mitigation measure against natural disasters such as floods, earthquakes, tsunamis, fault movements, rockfalls, debris flows, and avalanches (Brandl 2011; Fowze *et al.* 2012; Kuwano *et al.* 2012; Lambert and Bourrier 2013; Koseki and Shibuya 2014). The factors that foster the acceptance of GRS structures include aesthetics, reliability, low cost, simple and fast construction, seismic performance, and the ability to withstand large deformations. In practical design, the GRS structure is analyzed for internal, external, global, and seismic stability and deformation. In addition, the factors of safety (FS) against all failure modes are specified in design guidelines (Elias *et al.* 2001; Berg *et al.* 2009; NCMA 2010; AASHTO 2012). GRS structures are commonly categorized into reinforced soil walls (*i.e.,* GRS walls) and reinforced soil slopes (RSSs), differentiated by a facing inclination of 70°. This study focused on the internal stability of GRS walls.

For the internal stability design of GRS structures, design guidelines (Elias *et al.* 2001; Berg *et al.* 2009; AASHTO 2012) limit the use of limit equilibrium (LE) analysis for RSSs and the lateral earth pressure method for GRS walls. However, this limitation is somewhat arbitrary, and there is no theoretical reason why LE analysis cannot be extended to design GRS walls. In fact, the limitation of face inclinations should only be applied to the lateral earth pressure method but not to LE analysis because the lateral earth pressure method is theoretically based and is thus limited to retaining structures with small facing inclinations. The LE method is a popular and preferable approach for slope stability analyses of earth structures and natural slopes in practice due to its simple and well-established design procedures. Because the global slope stability of GRS walls still has to be evaluated using LE analysis, it would be more convenient and straightforward for engineers to conduct the internal stability design of GRS walls using LE analysis as well. A LE-based unified limit state design framework for GRS walls and slopes was proposed by Leshchinsky *et al.* (2014, 2017) and Xie *et al.* (2016). However, to date, limited studies have compared LE prediction with the physical test results of GRS walls (Probaha and Goodings 1996; Mane and Viswanadham 2010; Yang *et al.* 2013; Leshchinsky *et al.* 2014). The applicability and

Manuscript received February 26, 2019; revised August 5, 2019; accepted August 6, 2019.
[1] Associate Professor, Department of Civil Engineering, National Central University, Taiwan, R.O.C.
[2*] Professor (corresponding author), Department of Civil Engineering, National Taiwan University, Taiwan, R.O.C. (e-mail: khyang@ntu.edu.tw).
[3] Ph.D. Candidate, Department of Civil and Construction Engineering, National Taiwan University of Science and Technology, Taiwan, R.O.C.
[4] Ph.D., Department of Civil Engineering, National Central University, Taiwan, R.O.C.

suitability of LE analysis as a basis for the design of GRS walls require further validation.

For the deformation of GRS walls, design guidelines (Elias *et al.* 2001; WSDOT 2005; Berg *et al.* 2009; NCMA 2010; AASHTO 2012) provide anticipated values or specified tolerances for the maximum horizontal facing displacement of GRS walls. These recommended wall facing displacement values are empirically derived based on reinforcement type (*i.e.,* extensible or inextensible), reinforcement length, wall height, facing system, and surcharge. Bathurst *et al.* (2010) conducted a thorough review of current recommendations for the maximum horizontal facing displacement of GRS walls in numerous design guidelines and compared the recommended values with a database of reported deformations from high quality instrumented and monitored full-scale walls. They concluded that in most cases, FHWA and AASHTO recommendations provide reasonable upper limits for end-of-construction (EOC) movements for walls constructed on firm foundations. In practical design, no standard method exists for predicting facing deformations. Wall deformation is simply assumed to be within allowable limits, provided that the design meets the required FSs for GRS walls. Therefore, knowledge of the inherent FS of a GRS wall in correspondence to the recommended wall facing displacement values is valuable. In addition, the recommended wall facing displacement values in design guidelines are mostly applied for the wall deformation at EOC or under serviceability conditions. Little attention has been paid to wall deformation at failure (or just prior to failure), which provides a critical information for detecting incipient wall failure, and allows actions of early warning and response to be implemented before the final collapse of the wall.

The behavior of GRS walls has been evaluated extensively through monitored field tests and full-scale tests (Allen and Bathurst 2002, 2013, 2014a, 2014b, 2015; Bathurst *et al.* 2005, 2006, 2008, 2009a, 2009b; Kazimierowicz-Frankowska 2005; Yang *et al.* 2009, 2010, 2012; Miyata *et al.* 2015; Baral *et al.* 2016; Salem *et al.* 2018), centrifuge model tests (Goodings and Santamarina 1989; Porbaha and Goodings 1996; Springman *et al.* 1997; Chen *et al.* 2007; Mane and Viswanadham 2010; Balakrishnan and Viswanadham 2016; Costa *et al.* 2016; Ling *et al.* 2016), and numerical analyses (Ho and Rowe 1998; Rowe and Ho 1998; Ling *et al.* 2000; Rowe and Skinner 2001; Ling and Leshchinsky 2003; Hatami and Bathurst 2005, 2006; Guler *et al.* 2007; Huang *et al.* 2009, 2010; Damians *et al.* 2013, 2015; Mirmoradi and Ehrlich 2015; Sukmak *et al.* 2016; Yu *et al.* 2016a, 2016b, 2017; Salem *et al.* 2018). These studies have mainly: (1) investigated the effects of backfill materials, reinforcement arrangements, facing systems, foundation conditions, and compaction effects on the performance of GRS walls; (2) evaluated the mobilized reinforcement loads and distribution within GRS walls and compared them with various design methods for predicting reinforcement tensile loads. Due to the limitations of full-scale tests and numerical analysis, the majority of the aforementioned studies have focused on the performance of GRS walls under working stress (operational) conditions. Although these past studies provided useful information for the development of working stress design methods, studies on the GRS walls at failure, which provides valuable information to understand the failure mechanism, ultimate load carrying capacity, and pre-failure deformation characteristics of GRS walls, have not been fully investigated. Only a few studies have reported the failure mechanism of GRS walls by using centrifuge tests (Goodings and Santamarina 1989; Porbaha and Goodings 1996; Chen *et al.* 2007; Mane and Viswanadham 2010; Balakrishnan and Viswanadham 2016; Costa *et al.* 2016) and full-scale tests loaded with a substantial amount of surcharge (Bathurst *et al.* 2009b).

The preceding discussion motivated the authors to conduct a series of centrifuge model tests to study the performance of GRS walls under failure conditions and to evaluate the applicability of LE analysis for the internal stability design of GRS walls. The objectives of this study are to: (1) investigate the failure process and mechanism of GRS walls; (2) validate LE analysis as a basis for the internal stability design of GRS walls by comparing it with centrifuge test results; and (3) assess the facing displacement of GRS walls at failure. By combining the results of the centrifuge test and LE analysis, this study aims to establish the relationships between the FS and maximum horizontal facing displacement of GRS walls. The established relationships can then be used to identify the inherent FS of a GRS wall corresponding to the wall facing displacement values at EOC under serviceability conditions, as recommended in various design guidelines, and to determine wall deformation values at failure (FS = 1). This paper first introduces the centrifuge model tests conducted in this study. The soil and reinforcement materials, model preparation, and test procedure are discussed. The test results involving the failure process, failure mechanism, and deformation characteristics of GRS walls and the prediction of the failure conditions of GRS walls through LE analysis are then presented and discussed.

2. CENTRIFUGE TESTS

2.1 Centrifuge Model and Program

The centrifuge tests in this study were undertaken in the Centrifuge Modeling Laboratory of the Physical Modeling and Experimental Center at National Central University, Taiwan. A total of 10 centrifuge model tests with different reinforcement materials and wall heights, denoted as Tests 1 to 10, were conducted. Table 1 summarizes the centrifuge test program in the present study. Figure 1 shows schematic profile views of the GRS wall model. All models were constructed on a 150-mm firm foundation. The total height of the wall models varied from 224 to 320 mm, which included an additional layer (equal to reinforcement spacing S_v) of soil placed on the top of the wall to cover the topmost reinforcement layer. According to the centrifuge scaling law, the total wall heights were equivalent to $H = 8 \sim 24$ m in the prototype.

Regarding reinforcement layout, the reinforcement layer had a length L equal to 0.7 times of the wall height (*i.e.,* $L/H = 0.7$). Each reinforcement layer was folded back at the wall face and extended inward, forming a wrap-around facing and a secondary (overlapping) layer with length L_o equal to 40% of the primary reinforcement length. The number of reinforcement layers was $n = 16$ for all wall models; thus, the reinforcement spacing of the wall models ranged from $S_v = 10$ to 20 mm (equivalent to $0.4 \sim 1.4$ m in the prototype). To reduce particle size effects, Jewell (1993) suggested that the test specimen must be at least six times larger than the maximum particle size or 15 times larger than the average particle size of the soil. As listed in Table 1, the ratio of reinforcement spacing to mean particle size was kept sufficiently large ($S_v/d_{50} > 50$ for all wall models) to avoid the influence of particle size effects on the failure mechanism (*i.e.,* shear band formation) and test results.

Table 1 Geometrical configurations and test results of GRS wall models

Test No.	Geotextile type	T_{ult} (kN/m)	H (mm)	L (mm)	n	n_b	S_v (mm)	S_v/d_{50}	Test results		LE prediction	
									N_f (g)	θ (°)	N_f (g)	θ (°)
1	M1	0.10	256	168	16	21	16	57.1	26	61	24	60
2	M2	0.24	320	210	16	21	20	71.4	34	59	38	60
3	M2	0.24	288	190	16	21	18	64.3	45	58	46	59
4	M2	0.24	256	168	16	21	16	57.1	56	61	57	60
4a	M2	0.24	256	168	16	21	16	57.1	54	62	57	60
5	M2	0.24	224	147	16	21	14	50.0	64	63	75	61
6	M3	0.37	320	210	16	21	20	71.4	58	62	58	61
7	M3	0.37	288	190	16	21	18	64.3	72	65	71	62
8	M3	0.37	256	168	16	21	16	57.1	90	63	88	62
9	M4	0.40	320	210	16	21	20	71.4	65	57	62	59
10	M4	0.40	250	140	16	20	15	53.6	95	56	92	56

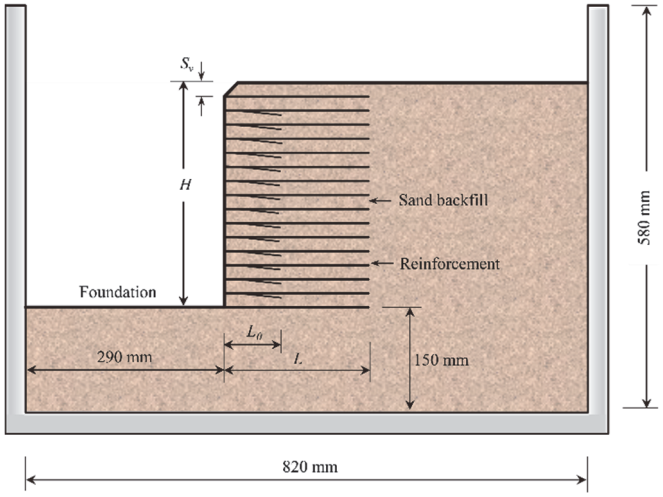

Fig. 1 Schematic profile view of centrifuge GRS wall model

2.2 Material Properties

The backfill of the wall models was uniform Fulung beach sand, which was classified as poorly graded sand (SP) according to the Unified Soil Classification System (USCS). The same soil was used for the retained fill and foundation. Figure 2 shows the soil grain size distribution curve. Table 2 summarizes the physical and mechanical properties of the soil. The test sand had a mean particle size d_{50} = 0.28 mm, coefficient of curvature C_c = 1.05, uniformity coefficient C_u = 1.78, minimum dry unit weight $\gamma_{d,\,min}$ = 13.3 kN/m^3, and maximum dry unit weight $\gamma_{d,\,max}$ = 15.9 kN/m^3 determined according to ASTM standards. The backfill of the wall models was prepared at a target relative density D_r = 70% by carefully pluviating sand from a hopper to achieve a state of uniform density. The corresponding soil unit weight was γ = 15.02 kN/m^3 at D_r = 70%. The soil shear strength properties obtained from a series of consolidated-drained triaxial compression tests were c = 0 kN/m^2 and ϕ_{tx} = 39.5°. The measured stress–strain-volumetric strain curves of the sand can be found in the study by Mohamed *et al.* (2014).

The importance of using plane strain strength to simulate the plane strain response of GRS walls was demonstrated by Hatami and Bathurst (2005, 2006) and Huang *et al.* (2009). In the present study, to characterize the shear strength of the sand under the plane strain conditions in the centrifuge model, the plane strain peak friction angle (ϕ_{ps}) was estimated using the correlation equation proposed by Lade and Lee (1976):

Table 2 Properties of soil used in the study

Soil properties	Symbol	Value
Basic soil parameters		
Unified Soil Classification System	USCS	SP
Specific gravity	G_s	2.66
Effective size (mm)	d_{10}	0.17
Mean particle size (mm)	d_{50}	0.28
Coefficient of curvature	C_c	1.05
Coefficient of uniformity	C_u	1.78
Minimum dry unit weight (kN/m^3)	$\gamma_{d,min}$	13.30
Maximum dry unit weight (kN/m^3)	$\gamma_{d,max}$	15.90
Unit weight of soil (kN/m^3)	γ	15.02
Relative density (%)	D_r	70
Strength properties		
Triaxial compression friction angle (°)	ϕ_{tx}	39.5
Plane strain peak friction angle (°)	ϕ_{ps}	42.3[a]

[a] Estimated based on the triaxial compression friction angle

$$\phi_{ps} = 1.5\,\phi_{tx} - 17 \quad (1)$$

where ϕ_{ps} and ϕ_{tx} are the friction angles under plane strain and triaxial compression conditions, respectively. Based on Eq. (1), the estimated plane strain friction angle was ϕ_{ps} = 42.3°, which was used for subsequent analyses in this study.

Four nonwoven geotextiles made of wood pulp, rayon, polyester and rayon, and polypropylene, denoted as M1, M2, M3, and M4, respectively, were used as reinforcement materials in the tests. Table 3 summarizes the properties of the four geotextile materials. A series of wide width tensile tests (ASTM D4595) was performed to evaluate the tensile strength properties of the geotextile materials. The ultimate tensile strengths of M1, M2, M3, and M4 obtained from the wide-width tests were T_{ult} = 0.06, 0.11, 0.17, and 0.25 kN/m at the ultimate strains of 8.5%, 29.7%, 10.9%, and 19.7%, respectively. These geotextile materials — having relatively low tensile strength — were selected with the intention of achieving wall failure in the centrifuge tests.

As a nonwoven geotextile is buried in soil, its tensile strength may be affected by soil confinement, which increases the confining pressure and restrains the lateral deformation (necking) of the geotextile. As a result, unconfined wide-width tensile tests may not accurately represent in-soil tensile strength values (Ling et al. 1992; Boyle *et al.* 1996). Studies have observed that the likely range for the in-soil tensile strength value of nonwoven geotextile is bound between the T_{ult} values obtained from wide-width and zero-span tensile tests (Christopher *et al.* 1986; Porbaha and Goodings

Table 3 Properties of four geotextile materials used in this study

Geotextile type	Material	Thickness (mm)	Ultimate strength, T_{ult} (kN/m)		Tensile stiffness, J_u[a] (kN/m)
			Zero-span test	Wide-width strip test	
M1	Wood pulp	0.07	0.10	0.06	0.71
M2	Rayon	0.13	0.24	0.11	0.37
M3	Polyester, Rayon	0.15	0.37	0.17	1.56
M4	Polypropylene	0.13	0.40	0.25	1.27

[a] calculated based on the wide-width strip test

1996a; Zornberg *et al.* 1998a; 1998b; Mohammed *et al.* 2013). Zornberg *et al.* (1998b) compared the breakage patterns in geotextile specimens tested using zero-span, wide-width, and centrifuge model tests. Test results revealed that the breakage pattern (a distinct rupture tear and no lateral necking) in the geotextile layer retrieved from the centrifuge slope model after the test resembled that of the geotextile tested using the zero-span test.

According to the proceeding discussion, zero-span tensile tests with clamps 6 mm apart were also performed in this study to properly characterize the reinforcement tensile behavior under the centrifuge test conditions (Christopher *et al.* 1986; Porbaha and Goodings 1996a; Zornberg *et al.* 1998a; 1998b). The ultimate tensile strengths of M1, M2, M3, and M4 obtained from the zero-span tests were T_{ult} = 0.10, 0.24, 0.37, and 0.40 kN/m, respectively. The T_{ult} values of the test geotextiles obtained from the zero-span test are approximately twice of those obtained from the wide-width tests (Table 3). The zero-span tensile strength values were used for subsequent analyses in this study and were verified by comparing them with the developed tensile force T_d values at failure back-calculated from LE analysis.

2.3 Model Preparation and Test Procedure

The wall models were constructed in a rigid aluminum container with the internal dimensions of 820 mm × 450 mm in the plan and a height of 580 mm. A transparent Plexiglas window was installed on one of the side walls of the container to enable in-flight observation of the wall model during test. To ensure that the wall model was tested under plane strain conditions, before constructing the wall model, thin plastic sheets with lubricant were applied at the internal faces of the container before constructing the wall model to minimize the boundary effects due to side friction between the soil and side walls.

At the beginning of model construction, a 150-mm-thick foundation was placed and compacted to achieve a dense state and prevent the occurrence of bearing capacity failure. After the foundation was placed, a temporary wooden formwork was assembled to provide lateral support for the wall model during construction. Thereafter, the wall model was constructed successively by installing a reinforcement layer, placing a soil layer with controlled density (D_r = 70%), and folding the geotextile back into the soil to provide a flexible wrapped facing. These processes were repeated until the wall model reached the desired height. The overlapping length of the topmost reinforcement was extended to the same distance of the primary reinforcement layer, and a layer of overburden soil (equal to S_v) was finally deposited on top of the wall to prevent the local pullout failure at this reinforcement layer.

The centrifuge testing procedure was divided into two stages. In the first stage, the wall model with the supporting wooden formwork was flew to a certain *g*-level until the measured settlement at the top of the wall was stable (to compress any voids through increasing self-weight) and then decelerated to a complete stop. In the second stage, the wooden formwork was removed and the models were loaded by gradually increasing the centrifuge acceleration in increments of 5g until failure of the wall model occurred. Each step of acceleration was maintained for 30s to ensure that the applied centrifugal force was completely transferred to the wall model at each step. During the centrifuge test, two couple-charged device (CCD) cameras, focusing on the side and the top of the model, were used to continuously monitor wall deformation and the development of cracks on top of the wall. The failure *g*-levels N_f of each test were recorded.

After wall failure was reached, the centrifuge was decelerated to a complete stop and each reinforcement sheet in the model was retrieved and pieced together to identify the breakage positions of the reinforcement. The location of the critical failure surface of the wall model was determined based on the observed tears (ruptures) in each reinforcement layer. Figure 3 shows typical photos of reinforcement layers retrieved from the dismantled wall models after completion of the test. Clear breaks observed from the retrieved reinforcement layers (as shown in Figs. 3(b) and 3(c)) indicated that the wall model failed internally when the reinforcements achieved their ultimate strength capacity. In addition, the nearly horizontal breakage pattern (perpendicular to the wall facing) in the reinforcement validated the plane strain condition in the centrifuge tests. A curved shape of the reinforcement tears would have been observed if significant boundary effects had occurred due to side friction.

2.4 Test Reproducibility

The reproducibility and consistency of the tests were verified by examining test results obtained under the same conditions. Figure 4 and Table 1 present a comparison of the test results of Tests 4 and 4a at wall failure. The white dashed lines in the inserted

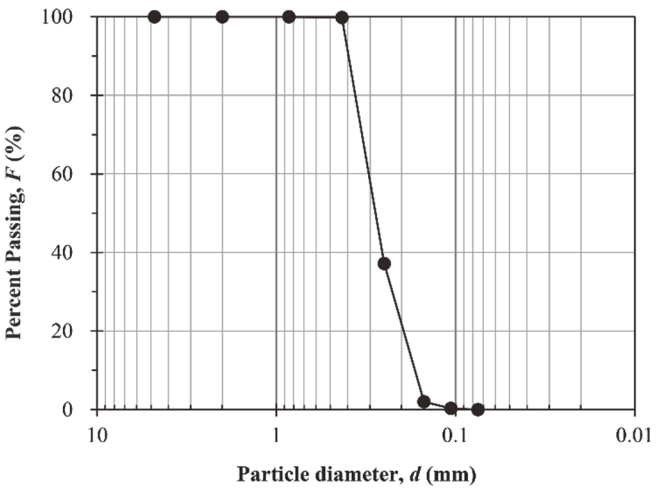

Fig. 2 Particle size distribution curve of the sand backfill

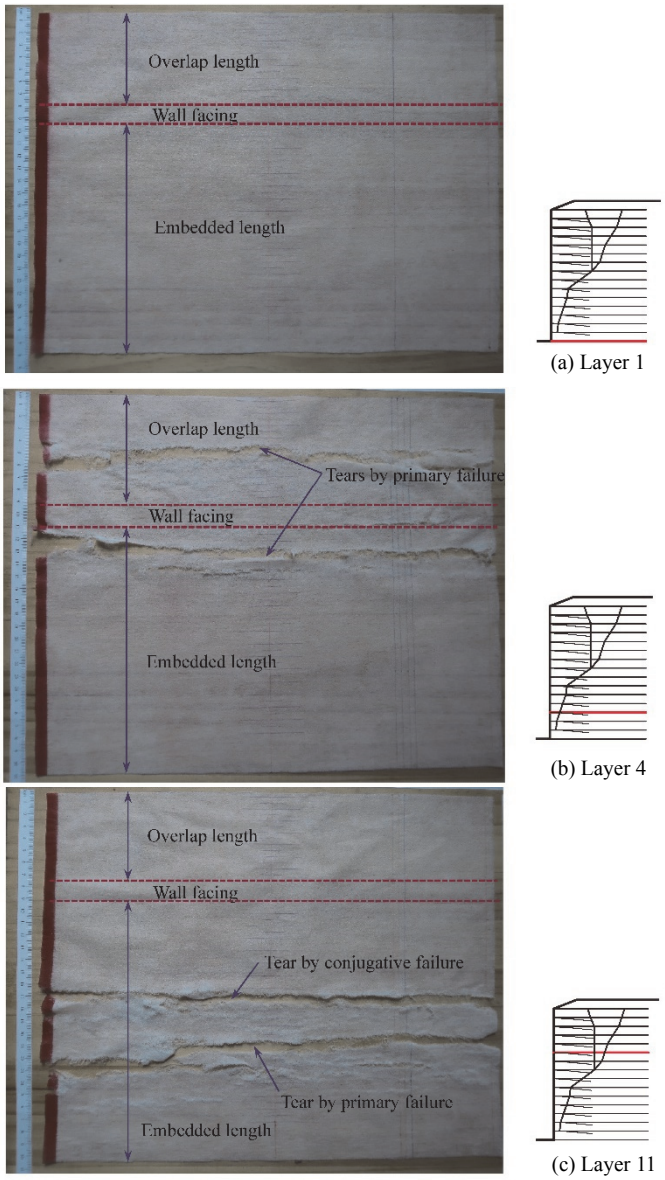

Fig. 3 Breakage pattern in reinforcement material after the wall failure: (a) Layer 1 (bottommost layer); (b) Layer 4; (c) Layer 11 (layer number increases from base to top of the model)

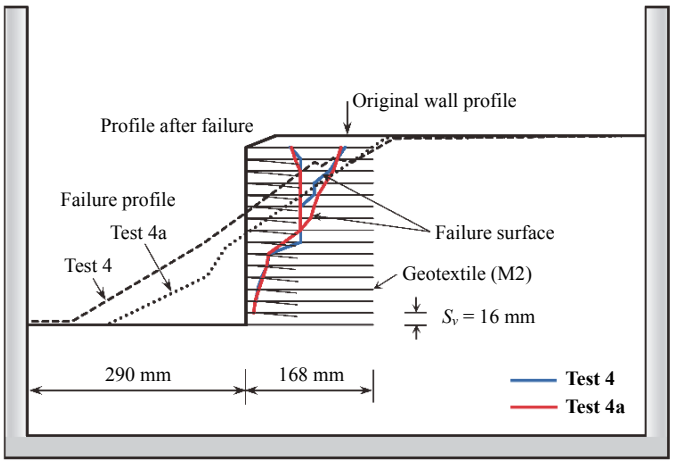

Fig. 4 Demonstration example of test reproducibility (Tests 4 and 4a)

photo in Fig. 4 indicate the original wall profile. The measured failure *g*-levels for Tests 4 and 4a (N_f = 56 and 54, respectively) were fairly close (Table 1). The failure occurred entirely within the reinforced zone in both tests. The developed failure surfaces of two tests matched well, and the final deposit profiles of failed soil mass were similar (Fig. 4). The comparison results demonstrate that the techniques of model preparation and test procedure adopted in this study can produce repeatable test results.

3. Wall Failure Mechanism

3.1 Failure Process

Figure 5 depicts a typical example of the failure process and development of failure surfaces of the GRS wall model observed from the centrifuge test. As the *g*-level increased, the wall gradually deformed. The wall facing displaced outward, and several settlement-induced transverse cracks, perpendicular to the direction of the facing displacement, developed at the top of the wall (Fig. 5(b)). When the *g*-level increased close to N_f (*i.e.,* at pre-failure stage), excessive settlement occurred, and a distinct subsidence developed at the top of the wall at the end of the reinforced zone (Fig. 5(c)). At the moment of failure, wall deformation suddenly increased, and the wall collapsed instantly.

The wall finally failed in two soil masses, which occurred almost simultaneously: the overturning of the first failure soil mass, followed by the sliding down of the second one (Fig. 5(c)). The two failure soil masses formed two (primary and conjugative) failure surfaces. The primary failure surface developed along an inclined plane, whereas the conjugative failure surface extended near vertically along the end of the overlapping length to the top of the wall. By observing the retrieved reinforcement layers, for the geotextile layers located toward the base of the wall (Fig. 3(b)), the failure surface intersected both the primary reinforcement layer and the overlapping length, indicating both primary and overlapping layers contributed to the system stability. For the geotextile layers located above the middle of the wall (Fig. 3(b)), the geotextile layer cut by the primary failure surface always displayed a clear tear, whereas the one intersected by the conjugative failure surface could show either a tear (Fig. 3(c)) or severe straining (without breakage). Figure 5(d) illustrates the final profile after the wall collapsed. The distance affected by the deposited failure soil mass was approximately 0.6 ~ 0.8 *H* away from the toe of the wall.

The failure process observed from the centrifuge tests in this study agree with the field observations obtained by Tatsuoka *et al.* (2000). They reported that the failure mode of flexible GRS walls (*i.e.,* without concrete facing) typically involved an excessive deformation and a development of a crack at the top of the wall, which in turn may trigger active wall failure.

3.2 Measured Failure *g*-Level and Failure Surface

Table 1 lists the measured failure *g*-level for all tests. The failure *g*-level N_f was defined at the moment when the rate of displacement at the crest of the wall suddenly increased. The determined failure moment matched well with the visual observation of the initiation of failure from the video taken by CCD cameras. Figure 6 shows the influence of reinforcement and wall geometric parameters on the measured failure *g*-level. An approximately linear relationship was observed between T_{ult} and N_f at a given wall

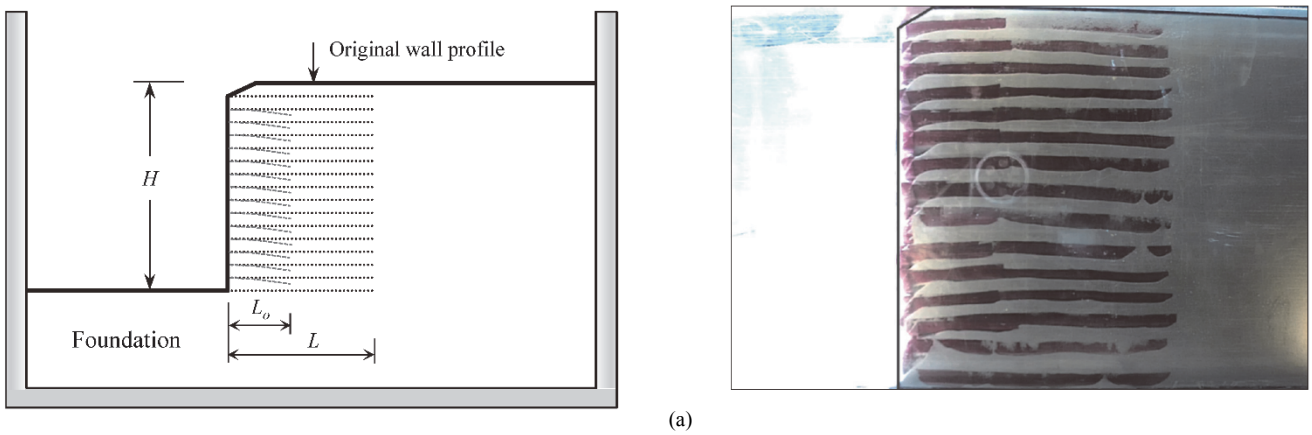

(a)

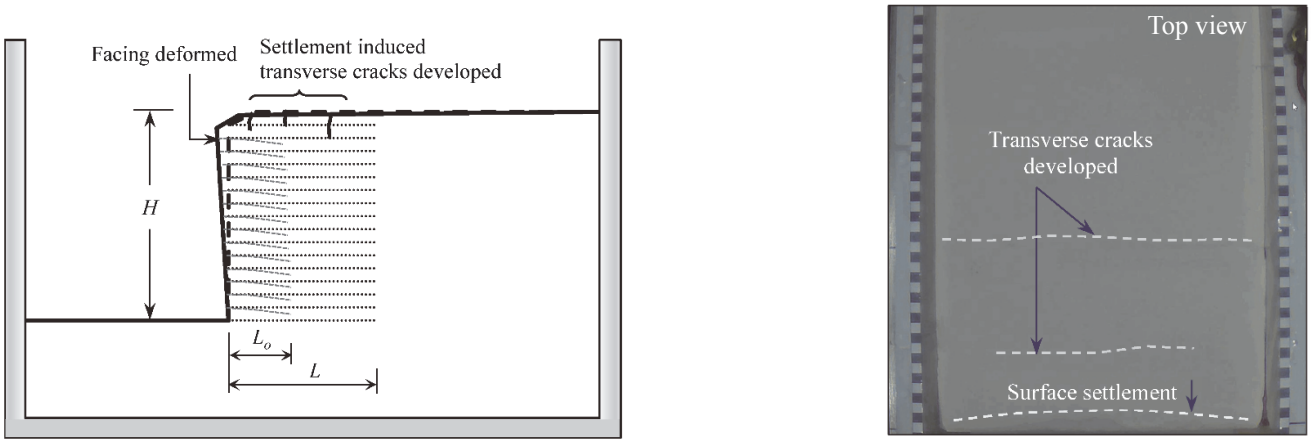

(b)

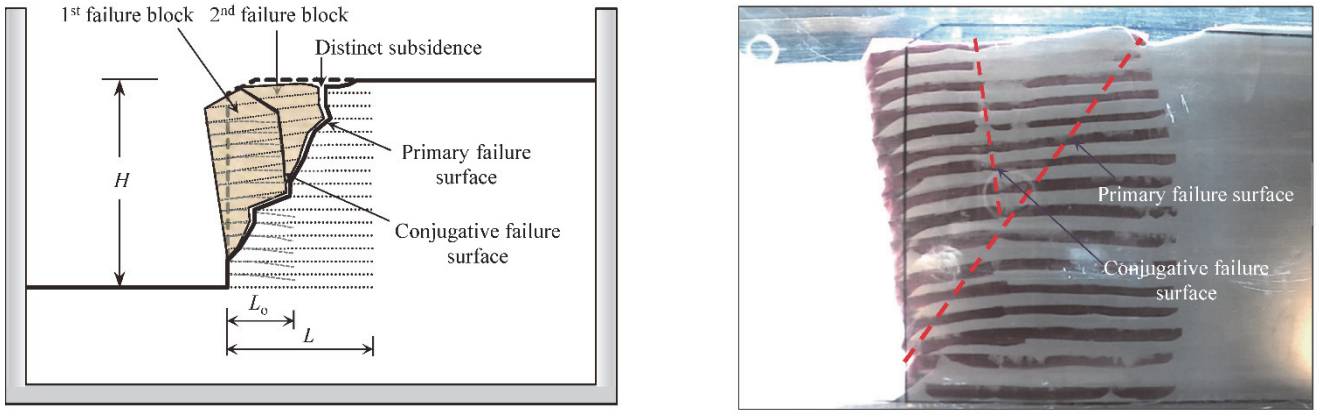

(c)

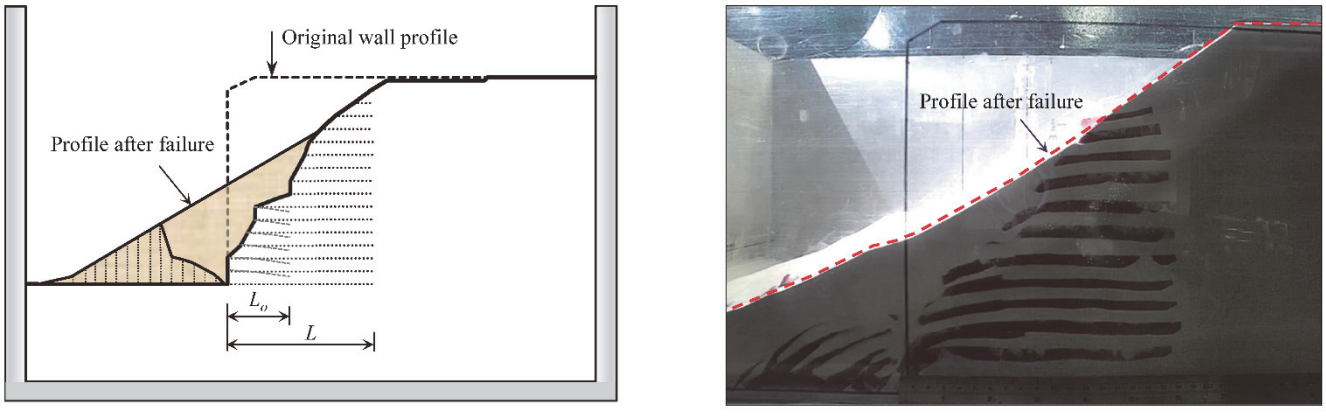

(d)

Fig. 5 Failure process of a GRS wall model: (a) initial stage; (b) increase of *g*-level; (c) at incipient failure; (d) after wall failure

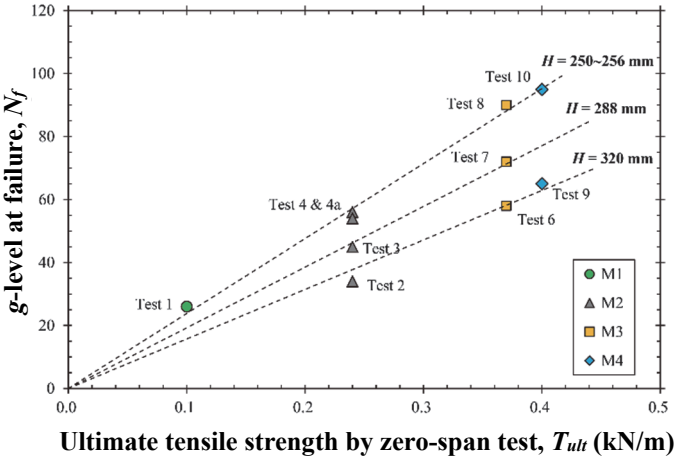

Fig. 6 Influence of reinforcement and wall geometric parameters on the measured failure *g*-level

height. The fitting line for each wall height passed through the origin of the figure. The linear relationships between T_{ult} and N_f for various wall heights clearly indicated that an increase in failure *g*-level corresponded to an increase in reinforcement tensile strength.

The effect of the wall height H on N_f was evaluated by comparing the slopes of the fitting lines. As expected, the slope of the fitting line increased as H decreased, implying the shorter wall model with the same reinforcement material failed at higher accelerations. Overall, the centrifuge test results suggest the reinforcement tensile strength and wall height have significant effects on the stability of GRS walls.

Figure 7 compiles the observed locations of the critical failure surfaces for all tests (only the primary failure surface is considered). Table 1 lists the inclination angle of the critical failure surfaces, ranging from θ = 56° to 65°, for all wall models. The location of the critical failure surface of the wall models appeared to

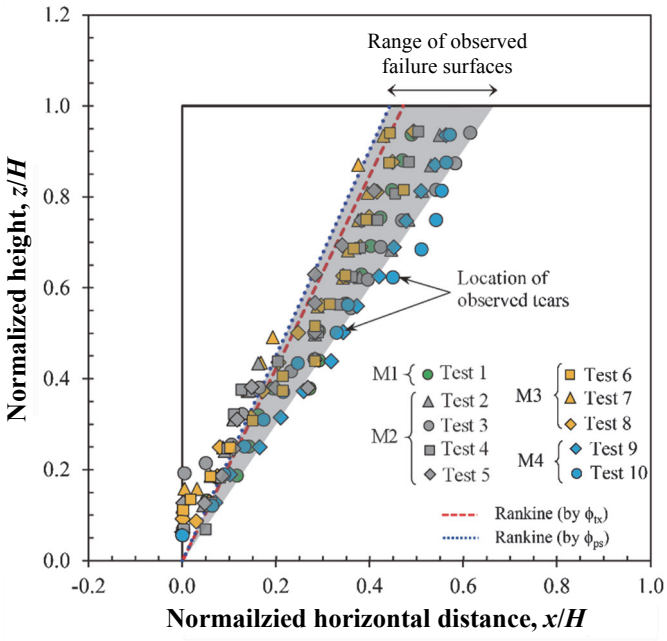

Fig. 7 Locations of critical failure surfaces measured from all centrifuge tests

be affected by the reinforcement inclusion. For instance, the failure surface of Tests 9 and 10 reinforced by geotextile M4, which has the highest tensile strength, had a low inclination angle. The upper limit of the critical failure surfaces of all tests was bounded by Rankine's theory (*i.e.,* tan (45° + ϕ/2)), resulting in the area of the active zone limited by the failure surface being close to or larger than that calculated by Rankine's theory.

Figure 7 also shows that the critical failure surfaces of all wall models passed through the wall face at the second reinforcement layer rather than through the toe of the wall at the first reinforcement layer. The observation of the retrieved reinforcement layers after the test demonstrated that the first (bottommost) reinforcement layers exhibited no evidence of tears and severe straining (Fig. 3(a)). This is likely because the boundary constraint from the dense foundation in the centrifuge models constrained soil movement as well as reinforcement deformation at the base of the wall model. As a result, the failure surfaces were prevented from passing through the wall toe. These results are consistent with the findings of studies on reinforced slopes by Zornberg *et al.* (1998a, 1998b). In addition, Allen *et al.* (2003) addressed similar attenuating effects of stiff competent foundations on reinforcement loads at the base of walls.

3.3 Equivalent Earth Pressure Coefficient

The influence of reinforcement and wall geometric parameters on the test results were combined and normalized into an equivalent earth pressure coefficient. Regarding the internal failure of GRS walls, at the moment of failure, the soil along the potential failure surface reached active failure, and all the reinforcement layers achieved the ultimate load as inferred from the centrifuge test results. The equilibrium relationships between horizontal soil stresses and reinforcement forces at failure can be further characterized by an equivalent earth pressure coefficient, K_T, defined as:

$$K_T(\phi,\beta)=\left(\frac{2n_b T_{ult}}{\gamma H^2}\right)\cdot\frac{1}{N_f} \tag{2}$$

where γ = unit weight of soil, H = wall height, n_b = number of broken reinforcement layers counting for both primary and overlap layers (listed in Table 1), T_{ult} = reinforcement ultimate tensile strength from zero-span test, and N_f = failure *g*-level. The K_T coefficient was first proposed by Zornberg *et al.* (1998b) for reinforced slopes. Based on the centrifuge test results for reinforced slopes, Zornberg *et al.* (1998b) found that the K_T value is only dependent on the backfill friction angle ϕ and facing inclination β but independent of reinforcement type and layout.

Figure 8 shows the normalized centrifuge test results and the comparison of the K_T value back-calculated from the centrifuge tests with the theoretical active earth pressure coefficient values. Because all the wall models had the same backfill (ϕ_{ps} = 42.3°) and facing inclination (β = 90°), a unique linear relationship was established between the normalized reinforcement tension summation and N_f. The K_T value (= 0.180) was calculated from the slope of the linear fitting line. The K_T value was slightly lower than the value obtained from Rankine's active earth pressure coefficient K_a (= 0.196). This discrepancy between K_T and K_a is likely because the soil-facing interface interaction in the wall models is not considered in the calculation of Rankine's K_a. Coulomb's K_a is further

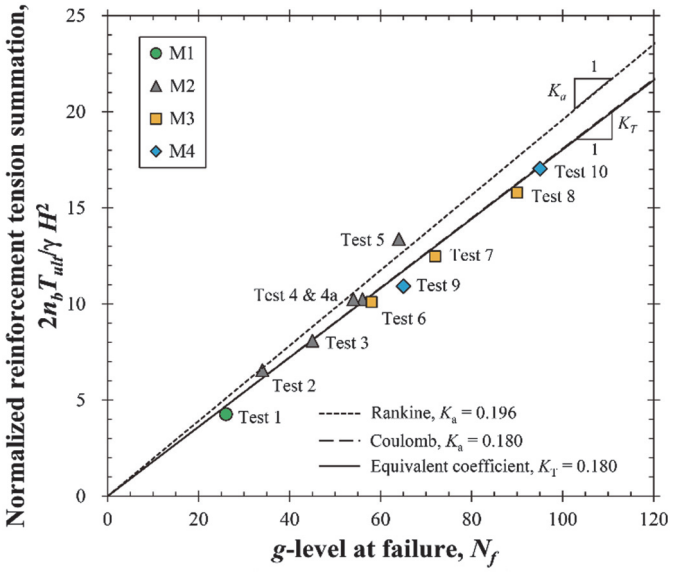

Fig. 8 Normalized centrifuge tests and the equivalent earth pressure coefficient

considered to account for the effect of soil-facing interface interaction. The comparison results in Fig. 8 indicate that the K_T value is consistent with the Coulomb's K_a value when tanδ/tanϕ = 0.6 (where δ is the soil-geotextile interface friction angle). Overall, the unique linear relationship established from the centrifuge test results confirms that the influence of the reinforcement and wall geometric parameters on the stability of GRS walls can be combined and normalized into a single K_T coefficient, and that the K_T value is comparable to the theoretical active earth pressure coefficients.

4. Limit Equilibrium Analyses

4.1 LE Model

In this section, LE analyses were performed to evaluate the applicability of LE analysis for GRS walls. Figure 9 presents the LE model and the search results for the critical failure surface and the corresponding FS value. In LE analyses, Spencer's method (Spencer 1967) — as coded in the slope stability program Slide v.7.0 (Slide 2017) — was adopted. Spencer's method is a rigorous slice method that satisfies all equilibrium conditions (*i.e.,* vertical force, horizontal force, and moment equilibrium) in each analyzed slope slice. Circular and noncircular failure surfaces were considered in this study. The noncircular failure surface comprised several piecewise linear segments. The search of critical failure surface was specified to initiate from the toe and exit at the top of the wall. The centrifugal force was simulated by increasing the unit weight of backfill until FS = 1 was obtained.

The shear strength of the sand in the centrifuge model was characterized by the plane strain friction angle. The geotextile was modeled as a reinforcement element by inputting a tensile force value. Figure 10 illustrates the input tensile force distribution along the primary reinforcement layer. The bilinear tensile force distribution along the reinforcement length was input based on its ability to provide rupture and pullout resistance. The rupture resistance was specified by inputting the T_{ult} value from the zero-span test. As the geotextile was wrapped around at the wall facing, the same T_{ult} value was assumed for the reinforcement tensile force at the wrapped facing by selecting the reinforcement anchorage function in the Slide program. The pullout resistance was calculated using the pullout equation:

$$P_r = R_c\, L_e (c_a + \sigma \tan\delta) \tag{3}$$

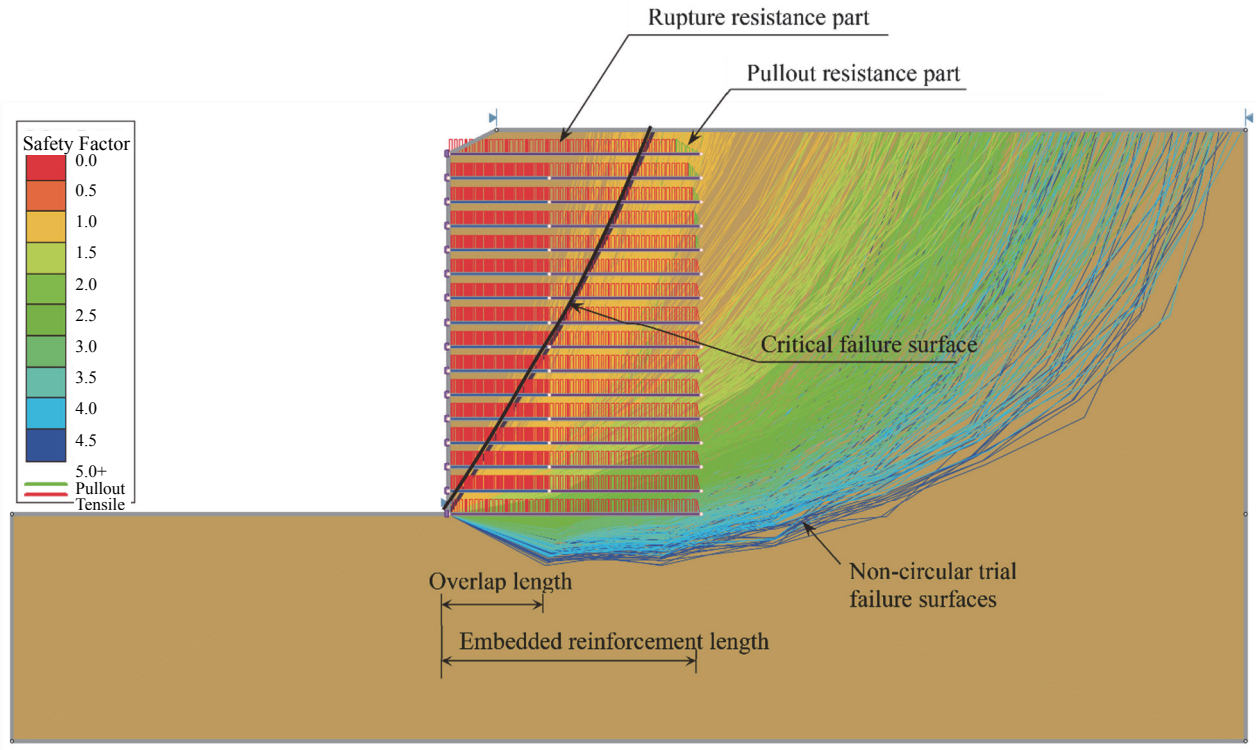

Fig. 9 LE model and LE results of the critical failure surface and the corresponding FS

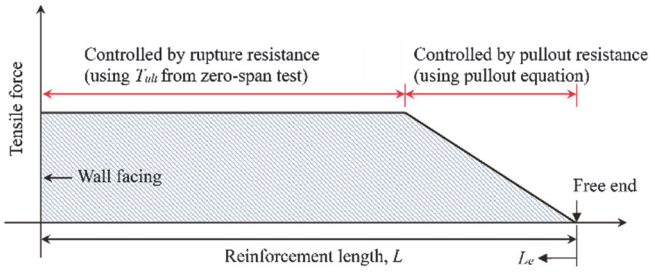

Fig. 10 Input tensile force diagram along reinforcement length

where P_r = pullout resistance; R_c = coverage ratio (= 2, considering both top and bottom surfaces of reinforcement according to the suggestions by AASHTO 2012 and Elias *el al.* 2001); L_e = horizontal distance to the free end of reinforcement; c_a and δ = interface cohesion and friction angle, respectively; and σ = effective overburden pressure on the reinforcement layer. The δ value was calculated using the interface efficiency factor tanδ/tanϕ = 0.6 (consistent with value used for calculating Coulomb's K_a in the previous section). As shown in Fig. 10, the pullout resistance of the reinforcement increased linearly from zero at the free end of the reinforcement to a value equal to the input T_{ult} value. The overlap layers were modeled as additional secondary reinforcement layers to account for the contribution of the geotextile overlaps to system stability. For simplicity, the tensile force was assumed to be uniformly distributed along the reinforcement length.

Modeling reinforcement tensile force distribution with depth requires certain assumptions, because the calculation problem is statically indeterminate when incorporating reinforcements into LE analysis. In this study, the rupture resistance part of the reinforcement tensile force was assumed to be uniformly distributed with depth (Fig. 9). The assumption of uniform tensile force distribution with depth is supported by the observations from experimental tests on GRS structures. Based on the measured reinforcement tensile strains from several well-instrumented full scale GRS walls, Allen and Bathurst (2002) and Allen *et al.* (2003) confirmed that the distribution of T_{max} versus normalized elevation of the wall is close to a uniform shape, especially at the middle part of the wall. Besides, based on the observation from centrifuge tests, Zornberg *et al.* (1998a) found that all reinforcement layers broke approximately at the same time at the moment of failure, suggesting the reinforcement tensile force with depth was uniformly mobilized and reached their ultimate tensile strength at the moment of failure. In addition, Zornberg *et al.* (1998b) and Mohamed *et al.* (2013) performed parametric studies to evaluate the influence of the reinforcement tensile force distribution with depth (*e.g.,* uniform, triangular, and trapezoidal distributions) for reinforced slopes and multi-tiered GRS walls, respectively. Both studies found the use of uniform distribution with depth yielded accurate LE results for predicting the failure *g*-levels and locations of critical failure surfaces. Finally, reduction factors such as creep, installation damage and degradation were not applied to the input reinforcement tensile force (*i.e.,* all reduction factors were 1.0). This is because unlike the field wall conditions, the wall models were carefully constructed to ensure that no installation damage occurred, and the duration of centrifuge tests was also kept sufficiently short to avoid long-term behavior such as creep or degradation.

4.2 Predicted Failure *g*-Level and Critical Failure Surface

The failure *g*-level and location of critical failure surface predicted by LE analyses were compared with the observed ones from the centrifuge tests. The accuracy of predicting failure *g*-level and identifying the critical failure surface are vital to the internal stability design of GRS walls against reinforcement breakage and pullout. Figure 11 shows the variation of FS with *g*-level for wall models with various geotextiles (Tests 1, 4, 8, and 9) calculated from LE analyses. In general, the FS values exhibited a nonlinear decreasing trend as the applied centrifugal accelerations increased. The predicted N_f value was then determined at the *g*-level corresponding to FS = 1, as indicated in Fig. 11 and in Table 1.

Figure 12 shows the comparison of the predicted and measured N_f for all centrifuge tests. Overall, the measured and predicted failure *g*-levels are in good agreement. The data points in Fig. 12 lie along the 1:1 line except for Test 5, which is slightly above the equality line. The overestimate of the N_f value in Test 5 is likely because the actual in-soil tensile strength of the geotextile is less than the input zero-span T_{ult} value. The in-soil tensile strength of the geotextile is evaluated and discussed in the next section.

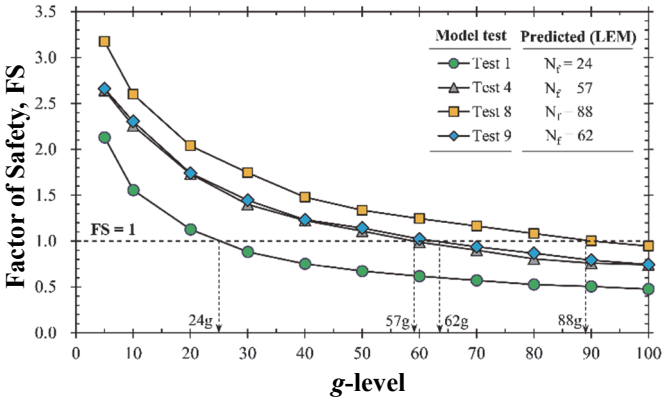

Fig. 11 Calculated factors of safety against *g*-level for various wall models

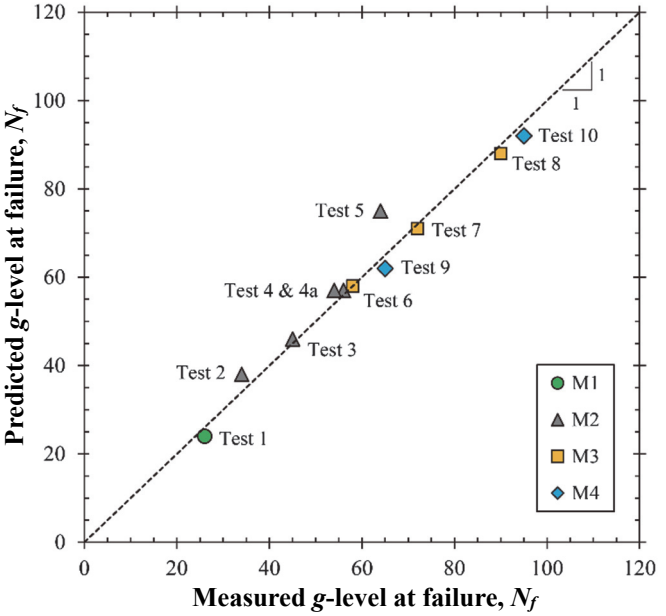

Fig. 12 Predicted and measured failure *g*-levels for all centrifuge tests

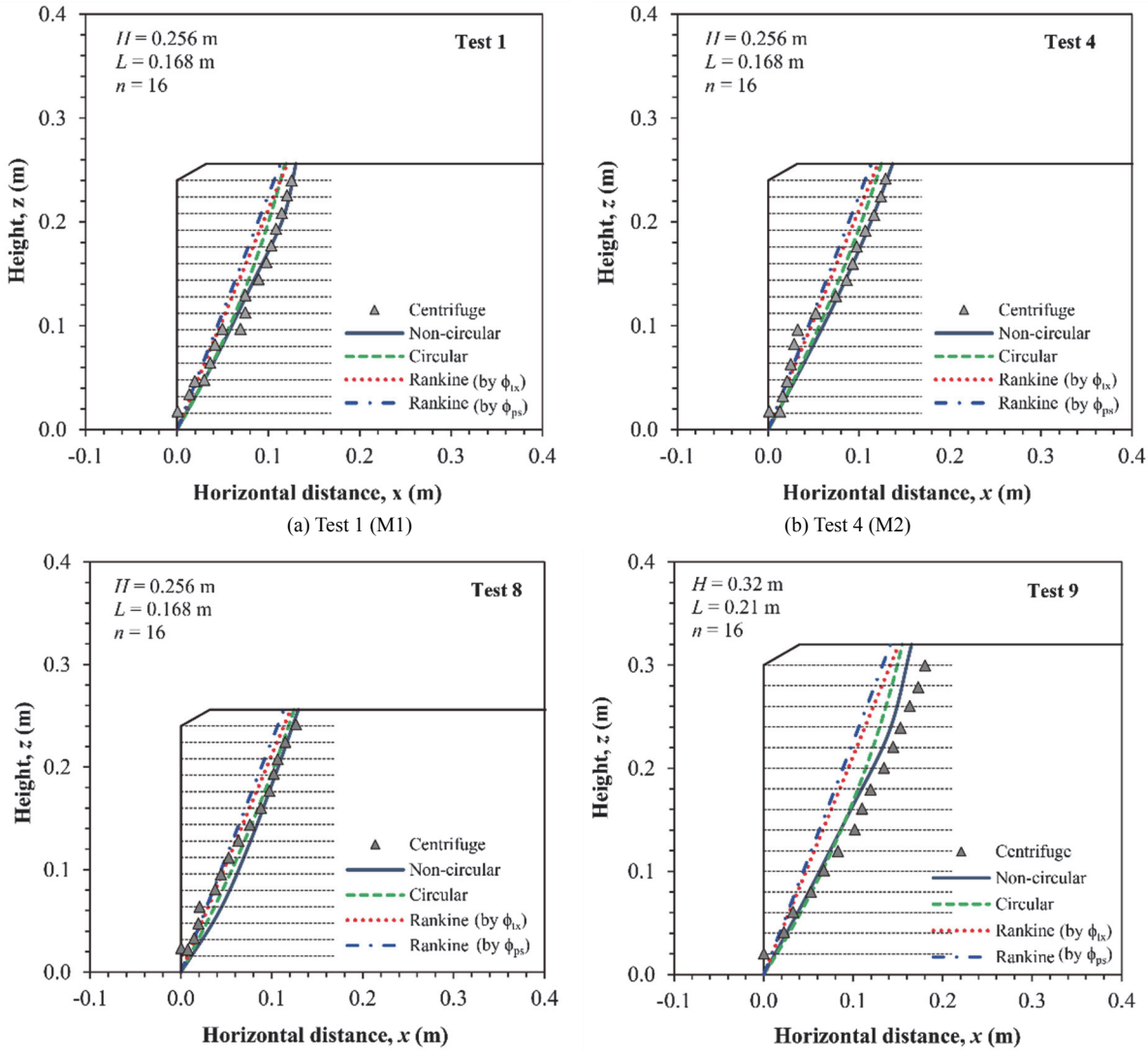

(a) Test 1 (M1) (b) Test 4 (M2)

(c) Test 8 (M3) (d) Test 9 (M4)

Fig. 13 Comparison of predicted and measured locations of critical failure surfaces

Figure 13 compares the locations of critical failure surfaces obtained from centrifuge tests and those predicted by LE analyses. The comparison results showed the critical failure surfaces predicted by LE analyses (both circular and noncircular) and those observed from the centrifuge tests were in good agreement for wall models with various reinforcement materials. Notably, the LE results indicated the critical failure surfaces of all the wall models only passed through the rupture resistance part rather than the pullout resistance part (as shown in Fig. 10), which was supported by centrifuged test result that no evidence of pullout was observed during and after the test. The centrifuge and LE results indicated the reinforcement length with L/H = 0.7 is sufficient to prevent reinforcement pullout failure.

The Rankine's failure surfaces suggested in design guidelines are also plotted in Fig. 13 for comparison. The observed locations of critical failure surfaces were reasonably predicted by Rankine's theory for the wall models with geotextiles M1 ~ M3 (Figs. 13(a) to 13(c)): the predicted and observed failure surfaces only differed slightly above the middle of the wall. However, an evident deviation in the Rankine's and observed failure surfaces was found for the wall models with geotextile M4, which has the highest tensile strength among four tested geotextiles (Fig. 13(d)). Overall, the LE analysis was more accurate in predicting the failure surface locations than Rankine's theory because the effect of reinforcement inclusion was considered in the LE calculation but not in Rankine's theory. The good match of the failure *g*-level and location of critical failure surface demonstrated that the LE method is competent at accurately predicting the failure conditions of GRS walls and validates the applicability and suitability of LE analysis for the internal stability design of GRS walls.

4.3 Evaluation of In-Soil Geotextile Tensile Strength

As mentioned previously, due to the influence of soil confinement, the ultimate tensile strength of geotextile in the centrifuge tests may differ from that measured from the unconfined wide-width tensile test and be close to that measured from the zero-span test. In this section, the use of the zero-span T_{ult} to represent the in-soil tensile strength in the centrifuge tests was verified through comparison with the developed reinforcement tensile force T_d value at wall failure. The T_d value at failure was back-calculated from LE analysis by adjusting the input tensile force value in LE analysis until FS = 1.0 was reached for each wall model.

Figure 14 shows the comparison of the T_d values at failure back-calculated by LE analyses and the T_{ult} values obtained from zero-span tensile tests. In Fig. 14, consistent T_d values were obtained for the wall models with the same reinforcement material, indicating the same type of the reinforcement developed a comparable amount of tensile forces, limited by its ultimate strength capacity, at wall failure. The back-calculated T_d values at failure were generally close to the zero-span T_{ult} values. Notably, the T_d value (= 0.21 kN/m) of Test 5 was slightly less than the zero-span T_{ult} value (= 0.24 kN/m) but still considerably larger than that obtained from the wide-width test (T_{ult} = 0.11 kN/m). This discrepancy indicated the actual in-soil tensile strength (or developed tensile force at failure) was less than the zero-span T_{ult} value, which may due to the less effect of soil confinement on the geotextile layers in Test 5 because the wall model in Test 5 was the shortest among all the tests. Overall, the comparison results are consistent with the findings of relevant studies (Christopher *et al.* 1986; Porbaha and Goodings 1996a; Zornberg *et al.* 1998a; 1998b; Mohammed *et al.* 2013). The satisfactory comparison results justify the use of the zero-span T_{ult} value in LE analyses for predicting the performance of GRS wall models at failure (*i.e.,* failure *g*-level and location of critical failure surface), providing adequate soil confinement is applied on geotextiles.

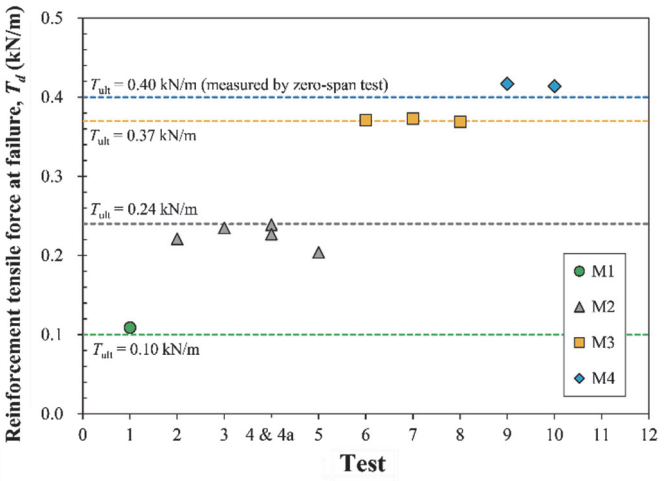

Fig. 14 Comparison of the developed reinforcement tensile force values at failure back-calculated by LE analyses with the ultimate tensile strength values measured from zero-span tests

5. Wall Deformation

5.1 Facing Displacement

The wall facing displacement is discussed in this section with special interests to investigate: (1) the inherent FS of a GRS wall corresponding to the wall facing displacement values under serviceability conditions as recommended in design guidelines; and (2) wall deformation at failure (or just prior to failure) as a crucial and detectable precursor of wall failure. Figure 15 shows the development of the total displacement at the wall crest with *g*-level for the wall models with various geotextiles. For comparison, the total displacement at the wall crest in Fig. 15 was normalized by wall height (*i.e.,* Δ/H). The test results revealed that the wall deformed progressively as the applied *g*-level increased. The total

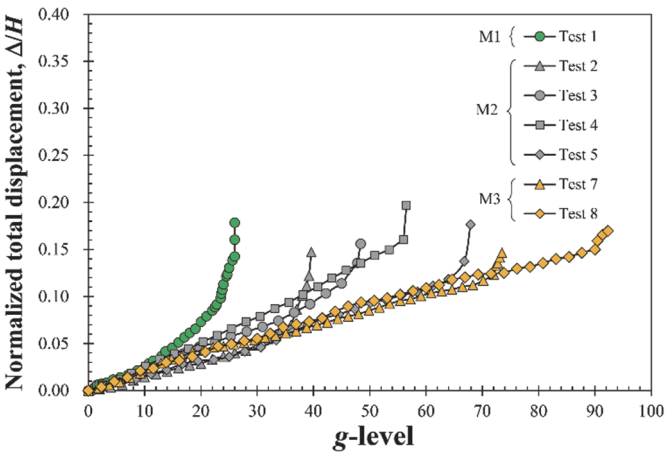

Fig. 15 Development of the total displacement at the wall crest with *g*-level

displacement and *g*-level exhibited a linear relationship before wall failure. At the moment of failure, wall deformation suddenly increased and the collapse of the wall occurred instantly. Because the sudden increase of deformation rate and collapse of the wall happened almost simultaneously, wall failure was classified as the catastrophic failure type.

A noticeable feature of the displacement data is that the total displacement curves of the wall models appear to follow the same trend at a small applied *g*-level (*i.e.,* under working stress conditions) and start to diverge at a large *g*-level. This is because the reinforcement requires sufficient deformation to mobilize its tensile force to effectively influence the performance of the wall model. Therefore, under the small *g*-level, wall deformation mainly depends on the deformation characteristics of the soil. Zornberg *et al.* (1998a) reported a similar observation that deformations in the centrifuge reinforced slopes were not sensitive to reinforcement characteristics and layout but rather depended mainly on the properties of the backfill soil.

Figure 16 shows the normalized horizontal facing displacement Δ_x profile at wall failure, which was determined at the moment prior to the sudden increase of the displacement rate. The wall model at failure exhibited a cantilever type of horizontal facing displacement profile, having a maximum displacement at the wall crest and decreased with the depth to zero displacement at the toe. The reinforcement material was found to influence the Δ_x value at failure. The Δ_x values at failure of the wall models reinforced by geotextiles with high tensile strength were less than those by geotextiles with low tensile strength because the strong and stiff reinforcement detained more horizontal displacement than the weak and ductile one.

Figure 17 shows the relationships between the normalized maximum horizontal facing displacements and FS for various wall models, established by combining Figs. 11 and 15. The maximum horizontal facing displacement $\Delta_{x,\,max}$ was defined as the maximum value along the Δ_x profile, which occurred at the wall crest as shown in Fig. 16. The factors of safety for various wall models were initially FSs = 2.5 ~ 3.0, and then nonlinearly decreased with $\Delta_{x,max}$. As indicated in Fig 17, the inherent factors of safety range from FSs = 1.5 ~ 2.5 for the GRS walls with L/H = 0.7 at EOC or under serviceability conditions corresponded to the anticipated values or specified tolerances of $\Delta_{x,max}$ recommended in several

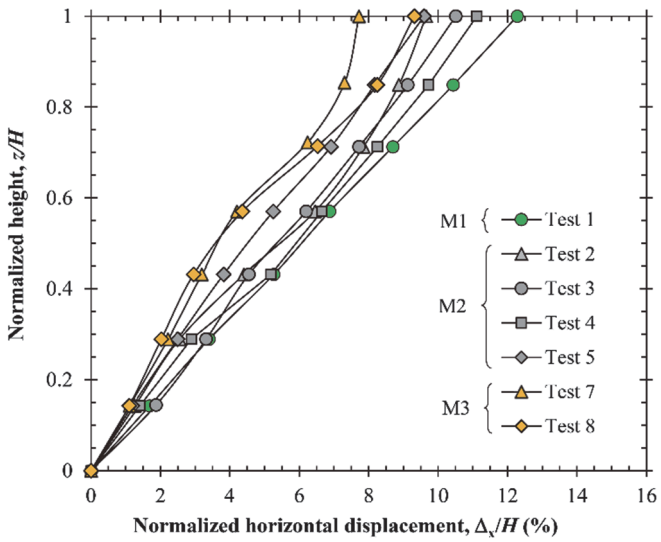

Fig. 16 Normalized horizontal facing displacement profile at incipient wall failure

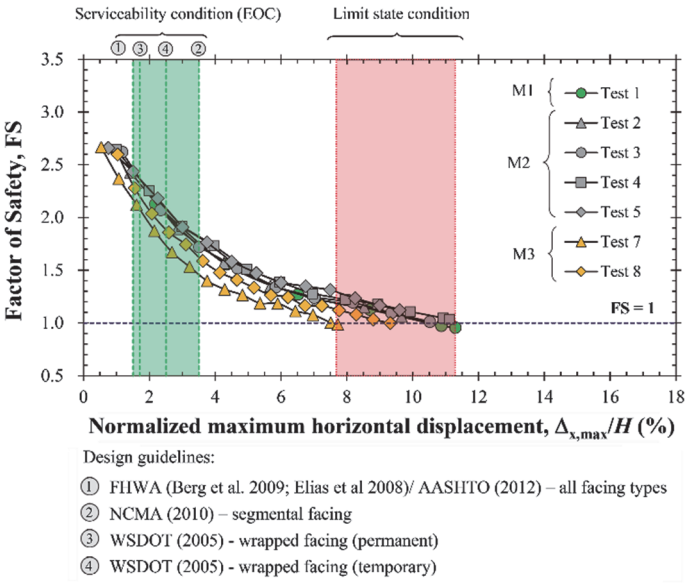

Fig. 17 Relationships between normalized maximum horizontal facing displacement and factor of safety

design guidelines (Elias *et al.* 2001; WSDOT 2005; Berg *et al.* 2009; NCMA 2010; AASHTO 2012). Notably, the presented FS values, calculated by LE analyses indicating the ratio of the available soil shear strength to the mobilized shear stress required for equilibrium, was different with the definition of FS against reinforcement breakage or pullout as specified in the design guidelines for the internal stability design of GRS walls. The $\Delta_{x,max}$ values reached 8% ~ 12% of H at incipient wall failure (FS = 1.0), which was, on average, approximately 4 ~ 5 times of the $\Delta_{x,max}$ values under the serviceability conditions recommended in design guidelines. The large wall displacement values measured at wall failure were due to the relatively weak and ductile geotextile materials used in the wall models compared with the ones used in real construction. The influence of geotextile materials on the wall facing displacement at failure is evaluated in next section.

5.2 Influence of Global Reinforcement Stiffness

Reinforcement parameters are expected to affect wall deformation. In this section, the influence of geotextile layout and stiffness in terms of global reinforcement stiffness S_{global} on the wall facing displacement at failure is evaluated. The S_{global} involves the effects of number of reinforcement layers and stiffness, computed as:

$$S_{global} = \frac{1}{H}\sum_{i=1}^{n} J_i \tag{4}$$

where J_i = secant tensile stiffness of the i^{th} reinforcement layer; n = number of reinforcement layers; and H = wall height. S_{global} was first proposed by Allen *et al.* (2003) in the K-stiffness method to predict the mobilized reinforcement tensile force of GRS walls under working stress conditions. The S_{global} was also used by Bathurst *et al.* (2010) to evaluate the influence of reinforcement parameters on wall facing displacement at EOC and under a 30 kPa surcharge. The trend of decreasing displacement with increasing S_{global} value was reported by Bathurst *et al.* (2010). In addition, they found the influence of compaction intensity was negligible after the walls were uniformly surcharged to 30 kPa pressure.

Figure 18 illustrates the influence of reinforcement global stiffness on the normalized maximum horizontal facing displacement at incipient wall failure. The horizontal deformation at failure of two other series of centrifuge model tests on GRS walls by Balakrishnan and Viswanadham (2016) and Chen *et al.* (2007) was also included for comparison. The backfill type and reinforcement layout and properties are summarized in Fig. 18. Because the selected two sets of centrifuge model tests in literature only reported the reinforcement tensile properties from wide-width tensile tests, all the S_{global} values in Fig 18 were consistently calculated by Eq. 4 using the secant tensile stiffness at failure strain J_u obtained from wide-width tensile tests. In addition to S_{global}, studies have demonstrated that the reinforcement length can influence the wall horizontal deformation (Mitchell and Christopher 1990; Chew *et al.* 1991; Rowe and Ho 1998; Bilgin and Kim 2010). The three sets of wall models shown in Fig. 18 were carefully selected to have L/H values close to 0.7. The influence of reinforcement length on the wall horizontal deformation is expected to be inconsequential according to Rowe and Ho (1998), who found that the wall horizontal deformation did not vary considerably for $L/H > 0.45$.

Figure 18 shows that the S_{global} had a significant influence on the maximum horizontal facing displacement of GRS walls at failure. The $\Delta_{x,max}/H$ values at failure ranged from 8% ~ 15% approximately at $S_{global} < 100$ kN/m^2, meaning that a large horizontal facing deformation could occur at wall failure for GRS walls with flexibly reinforcing systems. The $\Delta_{x,max}/H$ value of data SW1 obtained from Balakrishnan and Viswanadham (2016) is larger than those obtained in this study. This is likely because the soil deformability became actively influential (as indicated in Fig. 18, two sets of centrifuge tests have different backfill types) for flexibly reinforced GRS walls which have relatively less reinforcing effect. The $\Delta_{x,max}/H$ values at failure decreased as the S_{global} increased and appeared to converge to a single value (≈ 3.5%) when the S_{global} was approximately larger than 1000 kN/m^2, indicating that a small horizontal facing deformation could be expected at wall failure for GRS walls with stiffly reinforcing systems. Compared with the recommended wall facing displacement values in design guidelines (as indicated in Fig. 18), the difference between the $\Delta_{x,max}/H$ values

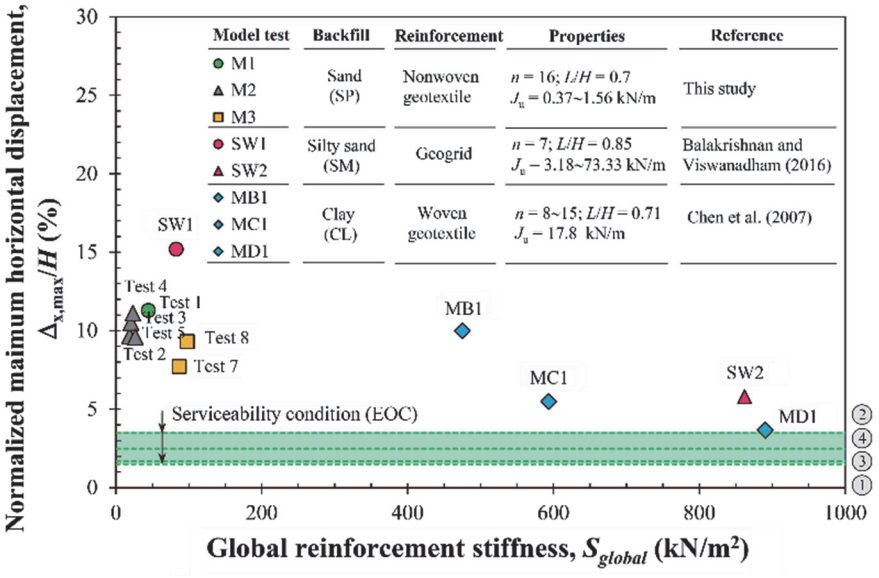

Fig. 18 Influence of global reinforcement stiffness on normalized maximum horizontal facing displacement at incipient wall failure (numbers in circles indicate the design guidelines listed in Fig. 17)

under working stress and failure conditions was profound at small S_{global} but became minor at large S_{global}. These comparison results indicate that when the wall status changed from working stress to failure conditions, for the flexibly reinforced GRS walls, the development of a noticeable wall deformation allowed actions of early warning and response to be implemented before the final collapse of the wall, whereas for the stiffly reinforced GRS walls, the wall could fail without showing evident symptoms of deformation.

6. CONCLUSIONS

A series of centrifuge tests was performed on the GRS walls with various reinforcement materials and wall heights to investigate the performance of GRS walls under failure conditions and to validate the applicability of LE analysis for the internal stability design of GRS walls. The failure process, failure mode (*i.e.,* failure *g*-level and location of the failure surface), wall facing displacement, and LE results were discussed. The conclusions drawn from this study are summarized as follows:

1. As the *g*-level increased, the wall facing gradually displaced outward, and several settlement-induced transverse cracks developed at the top of the wall. At pre-failure stage, excessive settlement occurred, and a distinct subsidence developed at the top of the wall at the end of the reinforced zone. At the moment of failure, wall deformation suddenly increased, and the collapse of the wall occurred instantly.
2. The centrifuge test results suggested the reinforcement tensile strength and wall height have significant effects on the stability (failure *g*-level) of GRS walls. The location of the critical failure surface of the GRS wall was affected by the reinforcement inclusion. The upper limit of the critical failure surfaces of all tests was bounded by Rankine's theory.
3. By back-calculating from the centrifuge test results, the influence of the reinforcement and wall geometric parameters on the stability of GRS walls could be combined and normalized into a single equivalent earth pressure coefficient K_T, and the K_T value was comparable to the theoretical active earth pressure coefficients.
4. The failure *g*-level and location of critical failure surface predicted by LE analyses were in good agreement with the observed ones from the centrifuge tests, demonstrating the applicability and suitability of LE analysis as a basis for the internal stability design of GRS walls.
5. Due to the influence of soil confinement, the developed tensile force T_d values at wall failure back-calculated from LE analysis were generally close to the ultimate tensile strength T_{ult} values obtained from the zero-span tests, and considerably larger than those obtained from the wide-width test. The consistent T_d values were obtained for wall models with the same type of the reinforcement, indicating the same type of the reinforcement developed a comparable amount of tensile forces at wall failure, which was limited by its ultimate strength capacity.
6. The total displacement and *g*-level exhibited a linear relationship before wall failure. The rate of displacement at the wall crest suddenly increased at the moment of failure. The wall model at failure exhibited a cantilever type of horizontal facing displacement profile. The reinforcement material affected the horizontal facing displacement value at failure: the strong and stiff reinforcement detained more horizontal displacement than the weak and ductile one.
7. The inherent factor of safety ranged from FS = 1.5 to 2.5 for wall deformation under serviceability conditions, as suggested in design guidelines. The maximum wall horizontal facing displacement $\Delta_{x,max}$ values reached 8% ~ 12% of the wall height at incipient wall failure (FS =1.0), which was, on average, approximately 4 ~ 5 times of the $\Delta_{x,max}$ values under serviceability conditions.
8. Compared with the wall deformation data in the literature, it was clearly observed that the global reinforcement stiffness S_{global} had a significant influence on the maximum horizontal facing displacement of GRS walls at failure. The $\Delta_{x,max}/H$ values at wall failure ranged from 8% to 15% for GRS walls with flexibly reinforcing system (approximately at S_{global} < 100 kN/m^2) and decreased close to 3.5% for GRS walls with stiffly reinforcing system (at $S_{global} \approx$ 1000 kN/m^2).

The findings and discussions in this study are based on the centrifuge test results of geotextile-reinforced soil walls with wrapped facings on firm foundations. The presented results may be relatively conservative for GRS walls with other facing types (*i.e.,* modular block or concrete panel facings) because, compared with other facing types, wrapped facing is less effective at improving system stability and detaining the facing displacement. In addition, the horizontal wall displacement depends on the wall geometry, ground water level, backfill soil properties, and foundation soil conditions, reinforcement properties, and reinforcement layout (length or spacing). Therefore, the established relationships between the FS and maximum horizontal facing displacement of GRS walls are only applicable to the conditions similar to the test conditions in this study. Further study can be conducted to investigate the influence of the aforementioned factors on the wall displacement.

FUNDING

The authors acknowledge the financial support of the Ministry of Science and Technology of Taiwan under grant number MOST107- 2628-E-002-003-MY3. The third and fourth authors also acknowledge the financial support for their Ph.D. studies provided by the Ministry of Education of Taiwan.

DATA AVAILABILITY

The data presented in this study are available from the corresponding author on reasonable request.

NOTATION

Basic SI units are given in parentheses

c_a	interface cohesion (°)
C_c	coefficient of curvature
C_u	coefficient of uniformity
d_{10}	effective grain size (mm)
d_{50}	mean particle diameter (m)
D_r	relative density (%)
FS	factor of safety
G_s	soil particle specific gravity
H	wall height (m)
J_u	secant tensile stiffness at failure strain (N/m)
K_a	active earth pressure coefficient
K_T	equivalent earth pressure coefficient
L	primary reinforcement length (m)
L_0	overlapping length (m)
n	number of reinforcement layers
n_b	number of broken reinforcement layers
N_f	failure *g*-level
S_{global}	global reinforcement stiffness (N/m^2)
S_v	reinforcement vertical spacing (m)
T_d	developed reinforcement tensile force at failure (N/m)
T_{ult}	ultimate tensile strength of reinforcement (N/m)
x/H	normalized distance from the facing
z/H	normalized elevation
x, z	coordinates (m)
β	facing inclination (°)
Δ	total displacement at wall crest (m)
Δ_x	horizontal facing displacement (m)
$\Delta_{x,\max}$	maximum horizontal facing displacement (m)
δ	interface friction angle (°)
γ	unit weight of the backfill (N/m^3)
θ	failure plane angle (°)
ϕ	friction angle (°)
ϕ_{ps}	plane strain peak friction angle (°)
ϕ_{tx}	triaxial compression peak friction angle (°)
σ	effective overburden pressure (N/m^2)

REFERENCES

AASHTO (2012). *AASHTO LRFD Bridge Design Specifications*., Sixth ed. American Association of State Highway and Transportation Officials., Washington, D.C, U.S.A.

ASTM D4595. *Standard Test Method for Tensile Properties of Geotextiles by the Wide-Width Strip Method*. American Society for Testing and Materials. West Conshohocken, PA, U.S.A.

Allen, T.M. and Bathurst, R.J. (2002). "Soil reinforcement loads in geosynthetic walls at working stress conditions." *Geosynthetics International*, **9**(5-6), 525-566. https://doi.org/10.1680/gein.9.0227

Allen, T.M., Bathurst, R.J., Holtz, R.D., Walters, D., and Lee, W.F. (2003). "A new working stress method for prediction of reinforcement loads in geosynthetic walls." *Canadian Geotechnical Journal*, **40**(5), 976-994. https://doi.org/10.1139/t03-051

Allen, T.M. and Bathurst, R.J. (2013). "Comparison of working stress and limit equilibrium behavior of reinforced soil walls." *ASCE Geotechnical Special Publication No. 230*, Sound Geotechnical Research to Practice, San Diego, California, United States, 500-514. https://doi.org/10.1061/9780784412770.033

Allen, T.M. and Bathurst, R.J. (2014a). "Design and performance of 6.3-m-high, block-faced geogrid wall designed using K-stiffness method." *Journal of Geotechnical and Geoenvironmental Engineering*, ASCE, **140**(2), 04013016. https://doi.org/10.1061/(ASCE)GT.1943-5606.0001013

Allen, T.M. and Bathurst, R.J. (2014b). "Performance of an 11 m high block-faced geogrid wall designed using the K-stiffness method." *Canadian Geotechnical Journal*, **51**(1), 16-29. https://doi.org/10.1139/cgj-2013-0261

Allen, T.M. and Bathurst, R.J. (2015). "Improved simplified method for prediction of loads in reinforced soil walls." *Journal of Geotechnical and Geoenvironmental Engineering*, ASCE, **141**(11), 04015049. https://doi.org/10.1061/(ASCE)GT.1943-5606.0001355

Balakrishnan, S. and Viswanadham, B.V.S. (2016). "Performance evaluation of geogrid reinforced soil walls with marginal backfills through centrifuge model tests." *Geotextiles and Geomembranes*, **44**(1), 95-108. https://doi.org/10.1016/j.geotexmem.2015.06.002

Baral, P., Bergado, D.T., and Duangkhae, S. (2016). "The use of polymeric and metallic geogrid on a full-scale MSE

wall/embankment on hard foundation: a comparison of field data with simulation." *International Journal of GeoEngineering*, **7**(1), 7-20. https://doi.org/10.1186/s40703-016-0035-6

Bathurst, R.J., Allen, T.M., and Walters, D.L. (2005). "Reinforcement loads in geosynthetic walls and the case for a new working stress design method." *Geotextiles and Geomembranes*, **23**(4), 287-322. https://doi.org/10.1016/j.geotexmem.2005.01.002

Bathurst, R.J., Miyata, Y., and Allen, T.M. (2010). "Facing displacements in geosynthetic reinforced soil walls." *Earth Retention Conference 3 (ER2010)*, ASCE Geo-Institute, Bellevue, Washington, United States, 42-459. https://doi.org/10.1061/41128(384)45

Bathurst, R.J., Miyata, Y., Nernheim, A., and Allen, A.M. (2008). "Refinement of K-stiffness method for geosynthetic-reinforced soil walls." *Geosynthetics International*, **15**(4), 269-295. https://doi.org/10.1680/gein.2008.15.4.269

Bathurst, R.J., Nernheim, A., and Allen, T.M. (2009a). "Predicted loads in steel reinforced soil walls using the AASHTO simplified method." *Journal of Geotechnical and Geoenvironmental Engineering*, ASCE, **135**(2), 177-184. https://doi.org/10.1061/(ASCE)1090-0241(2009)135:2(177)

Bathurst, R.J., Nernheim, A., Walters, D.L., and Allen, T.M. (2009b). "Inflence of reinfrocement stiffness and compaction on the performance of four geosynthetic-reinfroced soil walls." *Geosyntheitcs International*, **16**(1), 43-59. https://doi.org/10.1680/gein.2009.16.1.43

Bathurst, R.J., Vlachopoulos, N., Walters, D.L., Burgess, P.G., and Allen, T.M. (2006). "The influence of facing stiffness on the performance of two geosynthetic reinforced soil retaining walls." *Canadian Geotechnical Journal*, **43**(12), 1225-1237. https://doi.org/10.1139/t06-076

Berg, R., Christopher, B.R., and Samtani, N. (2009). *Design and Construction of Mechanically Stabilized Earth Walls and Reinforced Soil Slopes*. National Highway Institute, Federal Highway Administration, Washington, DC, U.S.A. https://www.fhwa.dot.gov/engineering/geotech/pubs/nhi10024/

Bilgin, O. and Kim, H. (2010). "Effect of soil properties and reinforcement length on mechanically stabilized earth wall deformations." *Earth Retention Conference 3 (ER2010)*, ASCE, Bellevue, Washington, United States, 556-563. https://doi.org/10.1061/41128(384)56

Brandl, H. (2011). "Geosynthetics applications for the mitigation of natural disasters and for environmental protection." *Geosynthetics International,* **18**(6), 340-390. https://doi.org/10.1680/gein.2011.18.6.340

Chen, H.T., Hung, W.Y., Chang, C.C., Chen, Y.J., and Lee, C.J. (2007). "Centrifuge modeling test of a geotextile-reinforced wall with a very wet clayey backfill." *Geotextiles and Geomembranes*, **25**(6), 346-359. https://doi.org/10.1016/j.geotexmem.2007.01.003

Chew, S.H., Schmertmann, G.R., and Mitchell, J.K. (1991). "Reinforced soil wall deformations by finite element method." *Performance of Reinforced Soil Structures*, McGown, E. A. ed., Thomas Telford, London., 35-40. https://www.icevirtuallibrary.com/doi/abs/10.1680/porss.16378.0006

Christopher, B.R., Holtz, R.D., and Bell, W.D. (1986). "New tests for determining the in-soil stress-strain properties of geotextiles." *Proceedings of the Third International Conference on Geotextile*, Vienna, Austria, 3, 683-686.

Costa, C.M.L., Zornberg, J.G., Bueno, B.S., and Costa, Y.D.J. (2016). "Centrifuge evaluation of the time-dependent behavior of geotextile-reinforced soil walls." *Geotextiles and Geomembranes*, **44**(2), 188-200. https://doi.org/10.1016/j.geotexmem.2015.09.001

Damians, I.P., Bathurst, R.J., Josa, A., and Lloret, A. (2015). "Numerical analysis of an instrumented steel-reinforced soil wall." *International Journal of Geomechanics*, ASCE, **15**(1), 04014037. https://doi.org/10.1061/(ASCE)GM.1943-5622.0000394

Damians, I.P., Bathurst, R.J., Josa, A., Lloret, A., and Albuquerque, P.J.R. (2013). "Vertical-facing loads in steel-reinforced soil walls." *Journal of Geotechnical and Geoenvironmental Engineering*, ASCE, **139**(9), 1419-1432. https://doi.org/10.1061/(ASCE)GT.1943-5606.0000874

Elias, V., Christopher, B.R., and Berg, R. (2001). *Mechanically Stabilized Earth Walls and Reinforced Soil Slopes Design and Construction Guidelines*. National Highway Institute, Federal Highway Administration, Washington, D.C.

Goodings, D.J. and Santamarina, J.C. (1989). "Reinforced earth and adjacent soils: Centrifuge modeling study." *Journal of Geotechnical Engineering*, ASCE, **115**(7), 1021-1025. https://doi.org/10.1061/(ASCE)0733-9410(1989)115:7(1021)

Guler, E., Hamderi, M., and Demirkan, M.M. (2007). "Numerical analysis of reinforced soil-retaining wall structures with cohesive and granular backfills." *Geosynthetics International*, **14**(6), 330-345. https://doi.org/10.1680/gein.2007.14.6.330

Hatami, K. and Bathurst, R.J. (2005). "Development and verification of a numerical model for the analysis of geosynthetic-reinforced soil segmental walls under working stress conditions." *Canadian Geotechnical Journal*, **42**(4), 1066-1085. https://doi.org/10.1139/t05-040

Hatami, K. and Bathurst, R.J. (2006). "Numerical model for reinforced soil segmental walls under surcharge loading." *Journal of Geotechnical and Geoenvironmental Engineering*, ASCE, **132**(6), 673-684. https://doi.org/10.1061/(ASCE)1090-0241(2006)132:6(673)

Ho, S.K. and Rowe, R.K. (1996). "Effect of wall geometry on the behaviour of reinforced soil walls." *Geotextiles and Geomembranes*, **14**(10), 521-541. https://doi.org/10.1016/S0266-1144(97)83183-4

Holtz, R.D., Christopher, B.R., and Berg, R.R. (2008). *Geosynthetic Design and Construction Guidelines*. *FHWA-NHI-07-092*. Federal Highway Administration, Washington, D.C.

Huang, B.Q., Bathurst, R.J., and Hatami, K. (2009). "Numerical study of reinforced soil segmental walls using three different constitutive soil models." *Journal of Geotechnical and Geoenvironmental Engineering*, ASCE, **135**(10), 1486-1498. https://doi.org/10.1061/(ASCE)GT.1943-5606.0000092

Huang, B.Q., Bathurst, R.J., Hatami, K., and Allen, T.M. (2010). "Influence of toe restraint on reinforced soil segmental walls." *Canadian Geotechnical Journal*, **47**(8), 885-904. https://doi.org/10.1139/T10-002

Jewell, R.A. (1993). "Links between the testing, modeling, and design of reinfroced soil." *Proceedings of International Symposium on Earth Reinforcement Practice*, Fukuoka, Japan, Balkema, 755-772.

Kazimierowicz-Frankowska, K. (2005). "A case study of a geosynthetic reinforced wall with wrap-around facing." *Geotextiles and Geomembranes*, **23**(1), 107-115. https://doi.org/10.1016/j.geotexmem.2004.05.001

Koseki, and Shibuya, S. (2014). "Mitigation of disasters by earthquakes, tsunamis, and rains by means of Geosynthetic-reinforced soil retaining walls and embankments." *Transportation Infrastructure Geotechnology*, **2**(1), 231-261. https://doi.org/10.1007/s40515-014-0009-0

Kuwano, J., Miyata, Y., and Koseki, J. (2012). "Performance of reinforced soil walls during the 2011 Tohoku earthquake." *Geosynthetics International*, **21**(3), 179-196. https://doi.org/10.1680/gein.14.00008

Lade, P.V. and Lee, K.L. (1976). *Engineering Properties of Soils*. Report UCLA-ENG-7652, University of California, Los Angeles, California.

Lambert, S. and Bourrier, F. (2013). "Desing of rockfall protection embankments: A review." *Engineering Geology*, **154**, 77-88. https://doi.org/10.1016/j.enggeo.2012.12.012

Leschchinsky, D., Leschchinsky, B., and Leschchinsky, O. (2017). "Limit state framwork for geosynthietc-reinforced soil structures." *Geotextiles and Geomembranes*, **45**(6), 642-652. https://doi.org/10.1016/j.geotexmem.2017.08.005

Leshchinsky, D., Kang, B., Han, J., and Ling, H. (2014). "Framework for limit state design of geosynthetic-reinforced walls and slopes." *Transportation Infrastructure Geotechnology*, **1**(2), 129-164. https://doi.org/10.1007/s40515-014-0006-3

Ling, H.I., Cardany, C.P., Sun, L.X., and Hashimoto, H. (2000). "Finite element study of a geosynthetic-reinforced soil retaining wall with concrete block facing." *Geosynthetics International*, **7**(2), 137-162. https://doi.org/10.1680/gein.7.0170

Ling, H.I. and Leshchinsky, D. (2003). "Finite element parametric study of the behavior of segmental block reinforced-soil retaining walls." *Geosynthetics International*, **10**(3), 77-94. https://doi.org/10.1680/gein.2003.10.3.77

Ling, H.I., Wu, J.T.H., and Tatsuoka, F. (1992). "Short-term strength and deformation characteristics of geotextiles under typical operational conditions." *Geotextiles and Geomembranes*, **11**(2), 185-219. https://doi.org/10.1016/0266-1144(92)90043-A

Ling, H.I., Xu, L., Leshchinsky, D., Collin, J.G., and Rimoldi, P. (2016). "Centrifugal modeling of reinforced soil retaining walls considering staged construction." *Geosynthetics, Forging a Path to Bona Fide Engineering Materials, Geo-Chicago 2016*, Hsuan, Y. G. ed., American Society of Civil Engineers, Chicago, Illinois, 95-105. https://doi.org/10.1061/9780784480182.009

Mane, A. and Viswanadham, B.V.S. (2010). "Centrifuge modeling of wrap-around geogrid-reinforced soil walls." *Indian Geotechnical Conference*, IGS Mumbai Chapter & IIT Bombay, 235-238.

Mirmoradi, S.H. and Ehrlich, M. (2015). "Modeling of the compaction-induced stress on reinforced soil walls." *Geotextiles and Geomembranes*, **43**(1), 82-88. https://doi.org/10.1016/j.geotexmem.2014.11.001

Mitchell, J.K. and Christopher, B.R. (1990). "North American practice in reinforced soil systems." *Proceedings of Conference on Design and Performance of Earth Retaining Structures*, P.C. Lambe and L.A. Hansen, Eds., ASCE Geotechnical Special Publication No. 25, Cornell University, Ithaca, NY, USA, 322-346.

Miyata, Y., Bathurst, R.J., and Miyatake, H. (2015). "Performance of three geogrid-reinforced soil walls before and after foundation failure." *Geosynthetics International*, **22**(4), 311-326. https://doi.org/10.1680/gein.15.00014

Mohamed, S.B.A., Yang, K.H., and Hung, W.Y. (2013). "Limit equilibrium analyses of geosynthetic-reinforced two-tiered walls: Calibration from centrifuge tests." *Geotextiles and Geomembranes*, **41**, 1-16. https://doi.org/10.1016/j.geotexmem.2013.08.004

Mohamed, S.B.A., Yang, K.H., and Hung, W.Y. (2014). "Finite element analyses of two tier geosynthetic-reinforced soil walls: Comparison involving centrifuge tests and limit equilibirum results." *Computers and Geotechnics*, **61**, 67-84. https://doi.org/10.1016/j.compgeo.2014.04.010

NCMA (2010). *Design Manual for Segmental Retaining Walls*, Bernardi, M., Ed., National Concrete Masonry Association, Herndon, Virginia, U.S.A.

Porbaha, A. and Goodings, D.J. (1996). "Centrifuge modeling of geotextile-reinforced cohesive soil retaining walls." *Journal of Geotechnical Enginnering*, ASCE, **122**(10), 840-848. https://doi.org/10.1061/(ASCE)0733-9410(1996)122:10(840)

Rowe, R.K. and Ho, S.K. (1998). "Horizontal deformation in reinforced soil walls." *Canadian Geotechnical Journal*, **35**(2), 312-327. https://doi.org/10.1139/t97-062

Rowe, R.K. and Skinner, D.G. (2001). "Numerical analysis of geosynthetic reinforced retaining wall constructed on a layered soil foundation." *Geotextiles and Geomembranes*, **19**(7), 387-412. https://doi.org/10.1016/S0266-1144(01)00014-0

Salem, M.A., Hammad, M.A., and Amer, M.I. (2018). "Field monitoring and numerical modeling of 4.4 m-high mechanically stabilized earth wall." *Geosynthetics International*, **25**(5), 545-559. https://doi.org/10.1680/jgein.18.00027

Slide (2017). *2D Limit Equilibrium Slope Stability Analysis*. Version. 7.0, Rocscience Inc., Toronto, Ontario, Canada. https://www.rocscience.com/

Spencer, E. (1967). "A method of analysis of the stability of embankments assuming parallel inter-slice forces." *Géotechnique*, **17**(1), 11-26. https://doi.org/10.1680/geot.1967.17.1.11

Springman, S.M., Balachandran, S., and Jommi, C. (1997). "Modelling pre-failure deformation behaviour of reinforced soil walls." *Geotechnique*, **47**(3), 653-663. https://doi.org/10.1680/geot.1997.47.3.653

Sukmak, K., Han, J., Sukmak, P., and Horpibulsuk, S. (2016). "Numerical parametric study on behavior of bearing reinforcement earth walls with different backfill material properties." *Geosynthetics International*, **23**(6), 435-451. https://doi.org/10.1680/jgein.16.00008

Tatsuoka, F., Tateyama, M., Tamura, Y., and Yamauchi. H. (2000). "Lessons from the failure of full-scale models and recent geosynthetic-reinforced soil retaining wall." *Proceedings of the Second Asian Geosynthetics Conference*, GeoAsia 2000, Kuala Lumpur, **1**, 23-53.

WSDOT (2005). *Geotechnical Design Manual*. M 46-03, Chapter 15 Abutments, retaining walls, and reinforced slopes, Washington State Department of Transportation, Olympia, Washington, U.S.A.

Xie, Y., Leschchinsky, B., and Yang, S. (2016). "Evaluating reinforcement loading with in surcharged segmental block reinforced soil walls using a limit state framwork." *Geotextiles and Geomembranes*, **44**(6), 832-844. https://doi.org/10.1016/j.geotexmem.2016.06.010

Yang, G.Q., Ding, J., Zhou, Q., and Zhang, B. (2010). "Field behavior of a geogrid reinforced soil retaining wall with a wrap-around facing." *Geotechnical Testing Journal*, **33**(1), 96-101. https://doi.org/10.1520/GTJ102410

Yang, G.Q., Liu, H., Lv, P., and Zhang, B.J. (2012). "Geogrid-reinforced lime-treated cohesive soil retaining wall: Case study and implications." *Geotextiles and Geomembranes*, **35**, 112-118. https://doi.org/10.1016/j.geotexmem.2012.09.001

Yang, G.Q., Zhang, B.J., Lv, P., and Zhou, Q.Y. (2009). "Behaviour of geogrid reinforced soil retaining wall with concrete-rigid facing." *Geotextiles and Geomembranes*, **27**(5), 350-356. https://doi.org/10.1016/j.geotexmem.2009.03.001

Yang, K.H., Utomo, P., and Liu, T.L. (2013). "Evaluation of force-equilibrium and deformation-based design approaches for predicting reinforcement tension within geosynthetics-reinforced soil structures." *Journal of GeoEngineering*, **8**(2), 41-54. https://dx.doi.org/10.6310/jog.2013.8(2).2

Yu, Y., Bathurst, R.J., and Allen, T.M. (2016a). "Numerical modeling of the SR-18 geogrid reinforced modular block retaining walls." *Journal of Geotechnical and Geoenvironmental Engineering*, ASCE, **142**(5), 04016003. https://doi.org/10.1061/(ASCE)GT.1943-5606.0001438

Yu, Y., Bathurst, R.J., Allen, T.M., and Nelson, R. (2016b). "Physical and numerical modelling of a geogrid-reinforced incremental concrete panel retaining wall." *Canadian Geotechnical Journal*, **53**(12), 1883-1901. https://doi.org/10.1139/cgj-2016-0207

Yu, Y., Bathurst, R.J., and Allen, T.M. (2017). "Numerical modelling of two full-scale reinforced soil wrapped-face walls." *Geotextiles and Geomembranes*, **45**(4), 237-249. https://doi.org/10.1016/j.geotexmem.2017.02.004

Zornberg, J.G., Sitar, N., and Mitchell, J.K. (1998a). "Performance of geosynthetic reinforced slopes at failure." *Journal of Geotechnical and Geoenvironmental Engineering*, ASCE, **124**(8), 670-683. https://doi.org/10.1061/(ASCE)1090-0241(1998)124:8(670)

Zornberg, J.G., Sitar, N., and Mitchell, J.K. (1998b). "Limit equilibrium as basis for design of geosynthetic reinforced slopes." *Journal of Geotechnical and Geoenvironmental Engineering*, ASCE, **124**(8), 684-698. https://doi.org/10.1061/(ASCE)1090-0241(1998)124:8(684)